JOURNAL OF MATERIALS SCIENCE 32 (1997) 1657–1663

Electron microscopy study of martensite in Cu–11.2 wt% Al–3wt% Ni

DELU LIU*, H. HASHIMOTO
Okayama University of Science, 700 Okayama, Japan
T. KO
Department of Material Physics, University of Science and Technology, Beijing, 100083 Beijing, People's Republic of China

The structures of martensites in a Cu–11.2 wt% Al–3 wt% Ni specimen, which was quenched from 1173 K, have been studied by high resolution electron microscopy (HREM) and diffraction techniques. Two kinds of martensites, i.e. β_1' and γ_1', coexisting adjacent to each other in the specimen were observed. The γ_1' matensite consists of microtwins with monoclinic structure. Three variants of the twin structure, i.e. $\{1\,2\,1\}$, $\{2\,1\,0\}$ and $\{1\,0\,1\}$ twins, are arranged within a single plate. The β_1' martensite possesses basically ordered *N*9*R* structure, but mixed with thin 2*H* domains. Some diffraction spots of this martensite shift along the [0 0 1] direction. In addition, extra weak reflections appear in the diffraction pattern due to heterogeneous atomic displacements. The microstructural features of the martensites are examined and discussed.

1. Introduction

The martensitic transformation in β Hume–Rothery phase alloys has been studied for more than 50 years. Progress in studying the transformation mechanisms and properties of the transformation products has provided scientific principles for various alloy designs. Associated theories have been proposed for the transformations in a wide range of materials [1–5]. It has been reported that β_1' and γ_1' martensites may form in a quenched Cu–Al or Cu–Al–Ni alloy containing 11–14 wt% Al. The β_1' martensite possesses an ordered 9*R* structure with stacking faults. While the γ_1' martensite consists of microtwins having an orthorhombic lattice with a Pnmm space group [1, 6–15], which is a *HCP* based superstructure (i.e. 2*H* structure). These martensites can transform to one another upon temperature or applied stress. Reverse transformations of the martensites have also been examined [16–21]. But more detailed observations and appropriate explanations are still required for the following considerations.

First, materials based on these types of transformation products have been implemented in various alloys and are still developing. A typical example is the shape memory effect and its applications [22–24, 27]. Thus a better understanding of the transformation mechanisms occurring in each case is needed.

Second, advances in high resolution analytical instruments and techniques, particularly the development of electron microscopy, have made it possible to observe directly the atomic structures of martensite and related interfaces. Electron microscope observations at the atomic level, especially *in situ* observations, are expected to shed new light into the field of solid phase transformations [25, 26].

Third, the growth mechanism in a wide range of plate- or lath-shaped transformation products, such as bainite, are closely related to the martensite transformation. It is important to clarify them [4].

In the present work a high resolution electron microscopy (HREM) investigation of martensites in a Cu–11.2 wt % Al–3 wt % Ni alloy is carried out and discussed.

2. Experimental procedure

Experimental alloys were melted in an induction furnace by using 99.9% pure metals of Cu and Al in an argon atmosphere. An ingot, 15 mm in diameter and 10 cm long, was heated at 1173 K for 24 h, then cut into discs of 0.5 or 1 mm thickness. Chemical analysis shows that the alloy composition is: 11.2 wt % Al, 3 wt % Ni and 85.1 wt % Cu. Homogenized alloy discs were reheated at 1173 K for 1 h in an argon atmosphere followed by quenching into iced brine. Afterwards these discs were thinned at room temperature by grinding before the final procedure of specimen preparation by ion beam milling at 4.5 kV with a beam current of 0.8 mA. Transmission electron microscopy (TEM) observations were carried out in a JEOL JEM 4000EX microscope operated at 400 kV.

*Permanent address: University of Science and Technology, Department of Material Physics, Beijing, 100083 Beijing, People's Republic of China.

0022–2461

3. Results and discussion

TEM observations in the present study show that two types of martensite structures coexist in the same specimen. One of them consists of microtwins, which is similar to γ_1' martensite in Cu–Al alloys [6–8]. The other structure has a large number of stacking faults within martensite plates: this structure resembles β_1' martensite in near eutectoid Cu–Al alloys [1, 11, 12]. The TEM micrograph given in Fig. 1 shows these two kinds of structures, where the regions marked G or B are martensites of the microtwin type and stacking fault type in the specimen, respectively. Each of these microstructures are discussed separately for convenience.

3.1. Structure of the γ martensite

The structure of the γ martensite observed in the present specimen was simulated by both X-ray and electron diffraction methods. The results are compared with γ_1' and β_1' structures from the literature. The unit cell of γ_1' martensite in the Cu–Al alloy and its relationship with the β_1 parent phase (DO_3 structure) is shown in Fig. 2 [1, 24]. By referring to the atomic structure of the Cu–Al alloy, it seems reasonable to assume that the lattice positions of the Al atoms would be at 0 0 0, 1/2 1/2 1/2, and Cu atoms at 0 1/2 0, 1/2 1/2 0, 1/2 3/2 0, 0 1/2 1/2, 0 3/2 1/2 and 1/2 0 1/2. Ni atoms are seen to occupy Cu atom sites [6–8]. A pair of electron micrographs, a bright field image and a dark field image of the $2\,0\,\bar{1}$ reflection of the martensite plate (G) at larger magnification, as well as its [0 1 0] zone diffraction pattern, are shown in Fig. 3. The diffraction pattern is indexed as in Fig. 3d. The lattice parameters obtained from this pattern (Fig. 3c) are $a = 0.44$ and $c = 0.42$ nm, whereas the angle between [1 0 0] and [0 0 1] is $\beta = 92°$. Nevertheless, the value of the lattice parameter b cannot be determined from Fig. 3c. It is clear from the diffraction pattern that the martensite plate (G) in Fig. 3 possesses a monoclinic lattice rather than an orthorhombic one.

X-ray diffraction experiments of the bulk specimens were also performed. The results can be accounted for by a monoclinic system with parameters: $a = 0.446$, $b = 0.540$, $c = 0.424$ nm and $\beta = 92°$. The calculated interplanar spacings, d, according to the above lattice parameters are listed in Table I. Those values resulting from X-ray diffraction experiments are also listed in the table for comparison. It seems that the calculated d values are consistent with the X-ray experimental results within reasonable error.

The diffraction pattern in Fig. 3c is actually a [0 1 0] zone pattern superposed upon its $(1\,0\,\bar{1})$ twin pattern, but the $(1\,0\,\bar{1})$ twin contrast is a little difficult to visualize on the micrographs of Fig. 3a and b because the $(1\,0\,\bar{1})$ planes are parallel to the incident beam. The twin reflection spots almost coincide with those of the matrix, but a small shift between them can be distinguished along certain directions, such as those pointed out by the arrows in Fig. 3d. The arrows M and N point at spots (2 0 1) and $(\bar{1}\,0\,\bar{2})_T$, and $(\bar{2}\,0\,\bar{1})$ and $(1\,0\,2)_T$, respectively. The subscript T denotes the twin reflection. The fine fringe contrast appearing in the bright and dark field images of Fig. 3a and b, respectively, will be discussed after the configuration of other two twin structures (i.e. {2 1 1} and {2 1 0} twins) is described.

Examples of the {2 1 1} and {2 1 0} twin structures observed in the γ martensite are shown in Fig. 4. Fig. 4a shows a TEM bright field image of γ martensite. The dark field image shown in Fig. 4b is formed by three superlattice spots $(\bar{2}\,1\,0)$, $(0\,\bar{2}\,1)_{T_1}$ and $(\bar{2}\,1\,1)_{T_2}$ [indicated by the circle labelled (B in the (1 2 4)* diffraction patterns (of Fig. 4d and e)]. Here the subscripts T_1 and T_2 denote the reflections from the $(2\,1\,\bar{1})$ and $(2\,\bar{1}\,0)$ twins, respectively. Fig. 4e gives the index pattern of Fig. 4d. Antiphase domains of this ordered γ martensite are clearly revealed in Fig. 4b, as shown by the arrows. Another dark field image shown in Fig. 4c is formed by the reflection $\bar{4}\,\bar{2}\,2$ and its twin spot, which are marked as A in Fig. 4d. In this picture the twin structure of the γ plates is also seen.

It can therefore be concluded that there are three variants of twin structures arranged in one martensite

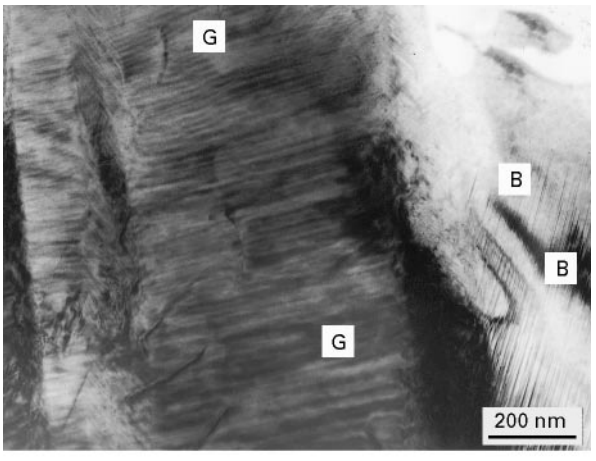

Figure 1 TEM micrograph of the quenched Cu–11.2 wt% Al–3 wt% Ni alloy showing two kinds of martensite plates: G (with microtwins) and B (with stacking faults).

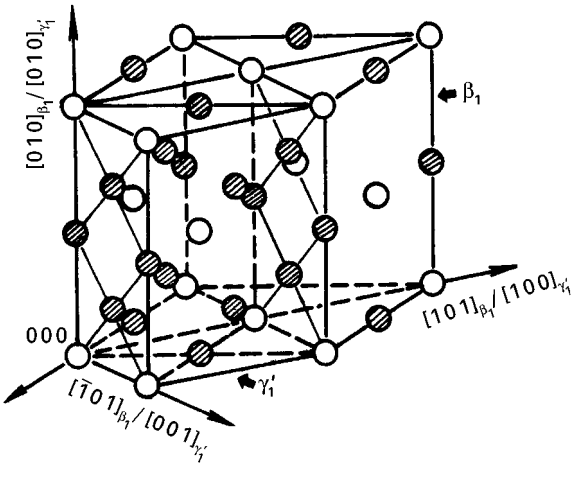

Figure 2 The structural model of γ_1' martensite in Cu–Al alloy and its relationship with the β_1 parent phase (DO_3 structure): (○) Al, (◍) Cu.

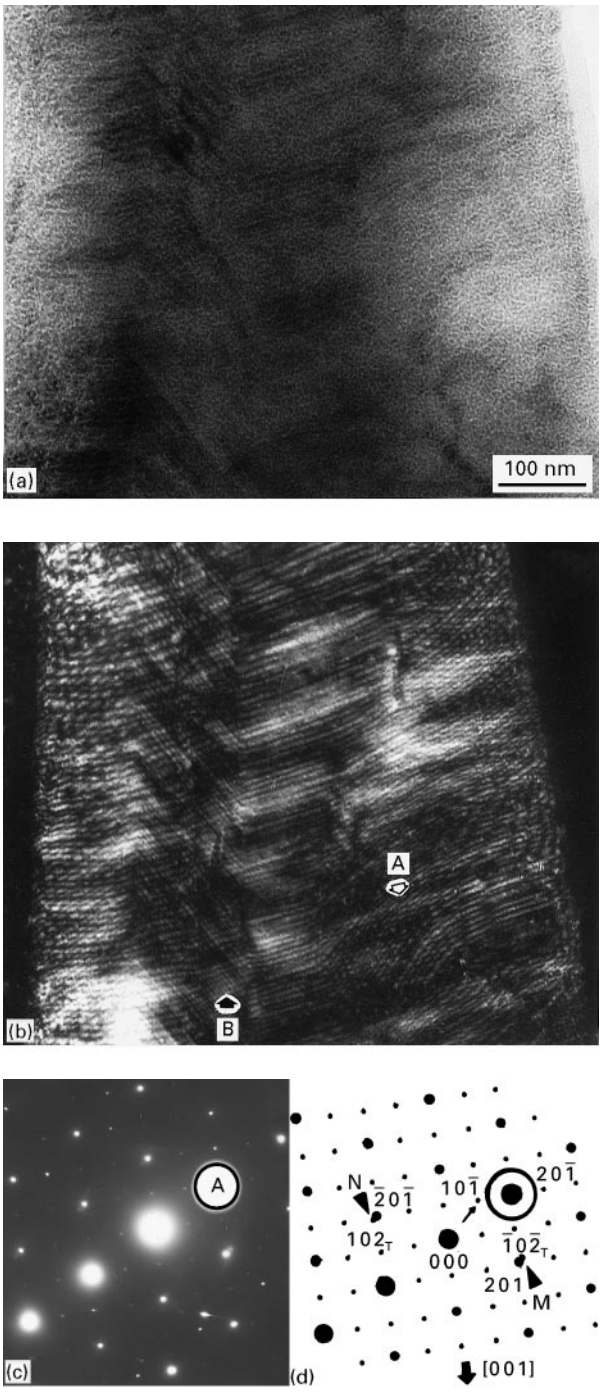

Figure 3 γ martensite in Cu–11.2 wt% Al–3 wt% Ni alloy. (a) TEM bright field image of a γ martensite plate. (b) central dark field image (CDF) of the same field as in Fig. 3a formed by the $(2\,0\,\bar{1})$ reflection (which is indicated by the circle labelled A on the diffraction pattern, Fig. 3c). The arrows at A and B point to the $(1\,0\,\bar{1})$ twin boundary traces and to the fringes formed by a series of $(2\,\bar{1}\,0)$ twins, respectively. (c) The [0 1 0] zone diffraction pattern of the martensite plate superimposed on the $(1\,0\,\bar{1})$ twin pattern. (d) Index of the [0 1 0] diffraction pattern of Fig. 3c; the arrows at M and N point to the (2 0 1) and $(\bar{1}\,0\,\bar{2})_T$ spots, where T denotes the twin reflections.

plate as shown in Fig. 5. The fringe contrast shown in Fig. 3b can be due to the above array of twin structures. In certain orientations, such as in the case of Fig. 3b, the $(1\,0\,\bar{1})$ twin boundaries are parallel to the incident beam: their contrasts in the image are straight lines. An example of the $(1\,0\,\bar{1})$ twin boundary trace is shown by arrow A in Fig. 3b. However, the $(2\,1\,\bar{1})$ twin boundaries give rise to curve fringe contrast in the

TABLE I Interplanar spacing, *d*, values obtained from X-ray diffraction (experimental) and calculated for γ_1' and β_1' martensite, respectively, in the Cu–11.2 wt % Al–3 wt % Ni sample quenched from 1173 K

Experimental ($nm \times 10^{-1}$)	Calculated for γ_1'		Calculated for β_1'	
	h k l	*d*	h k l	*d*
3.4026			1 1 1	3.382
3.2845			0 1 9	3.286
			1 0 8	3.271
2.2295	2 0 0	2.229	2 0 2	2.230
			1 2 2	2.231
2.1192	0 0 2	2.119	0 0 1 8	2.112
1.9862			2 0 8	2.032
1.9404	2 0 1	1.945	1 2 1 0	1.937
1.6340			1 2 1 6	1.634
1.6020	$2\,2\,\bar{1}$	1.608	0 3 9	1.600
1.5884			2 2 8	1.600
1.5781	2 2 1	1.578		
1.5377			2 2 1 0	1.551
1.4733			3 0 0	1.497
1.3968			2 2 1 6	1.384
1.3635			3 1 9	1.362
1.3611				
1.3530	2 2 2	1.353		
1.3215	2 2 2	1.318		
1.3006			0 4 0	1.298

[a]The *d*-values are calculated according to lattice parameters: $a = 0.446$ nm, $b = 0.540$ nm, $c = 0.424$ nm, $\beta = 92^\circ$, $\alpha = \gamma = 90^\circ$.
[b]The lattice parameters are: $a = 0.449$ nm, $b = 0.519$ nm, $c = 3.82$ nm, $\alpha = \beta = \gamma = 90^\circ$.

picture because they are inclined with respect to the electron beam, and the intersections with the surface of the specimen are curved due to changes in thickness of the specimen. The fringes shown by arrow B in Fig. 3b are due to a series of $(2\,\bar{1}\,0)$ twins. This geometrical configuration of different twins can also be observed along other crystallographic orientations.

3.2. Martensite with stacking faults

β_1' martensite is also observed in the specimen marked B in Fig. 1, which contains a large number of stacking faults. At larger magnification, a region of plate B, normal to its [0 1 0] zone axis, and its diffraction pattern are given in Fig. 6a and b, respectively. Comparison of this pattern with the (0 1 0)* pattern of an ordered 9*R* structure indicates that they basically coincide with each other [1, 12, 28], but in the present work some reflection spots are shifted along the [0 0 1] direction. A portion of the (0 1 0)* diffraction pattern is enlarged and is shown in Fig. 6c. It can be seen that many weak reflection spots appear every two main spots; this is more clearly seen at larger magnification between spots 2 0 2 and 2 0 8 in Fig. 6c. This implies that there is certain periodicity of the atomic stacking in this structure.

A high resolution image of the martensite plate (B) projected along the [0 1 0] orientation is given in Fig. 6d. A number of stacking faults can be seen, examples of them are shown by the arrows labelled S. These stacking fault planes (i.e. the close-packed $(0\,0\,1)_{9R}$ plane in an ordered 9*R* structure) are perpendicular to the image plane, which is parallel to the

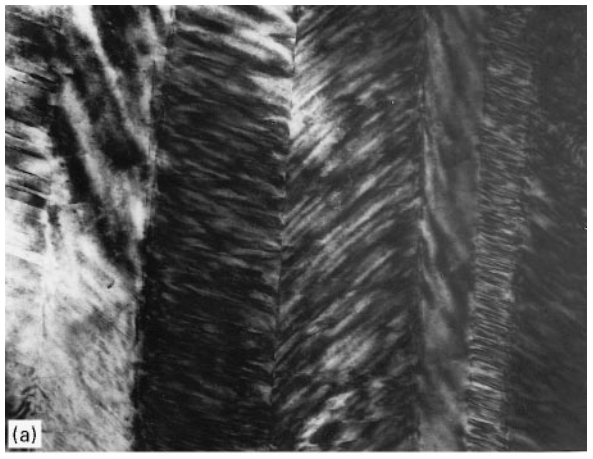

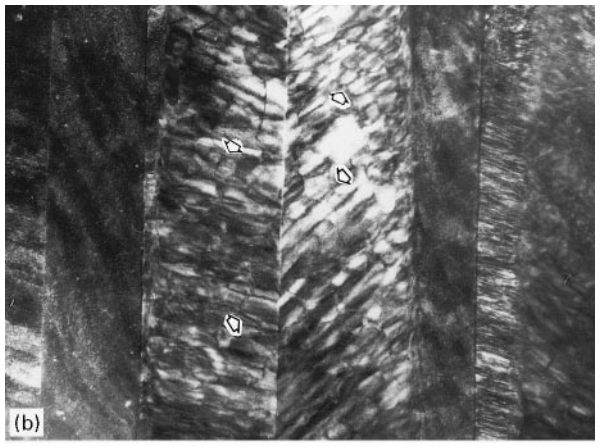

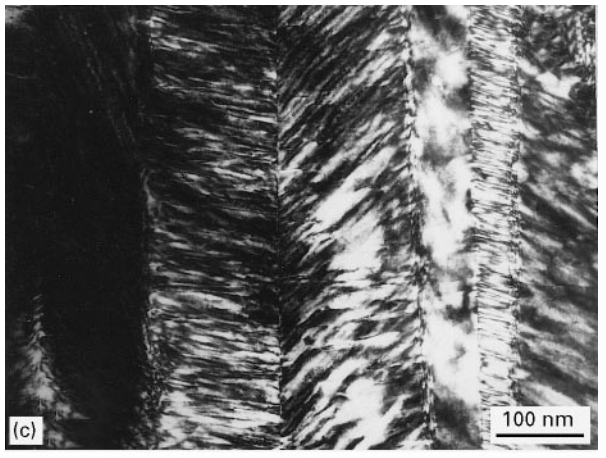

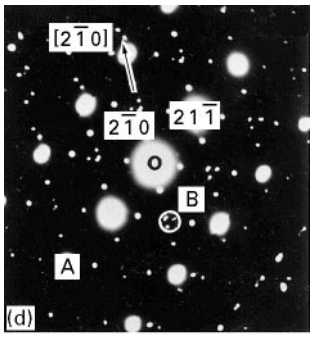

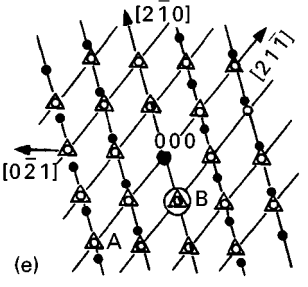

Figure 4(a) TEM bright field image of the γ martensite in the specimen. (b) Dark field image of the same area as shown in Fig 4a, formed by reflections (indicated by the circle labelled B shown in the diffraction patterns in Fig. 4d and e). Antiphase domain boundaries are indicated by arrows. (c) Dark field image of the reflections (marked A in Fig. 4d). (d) Diffraction pattern (1 2 4)* of the γ martensite. (e) Index of the (1 2 4)* diffraction pattern (△) with [2 1 1̄] (○) and [2 1̄ 0] twin (●) patterns. The remaining spots are due to secondary diffraction.

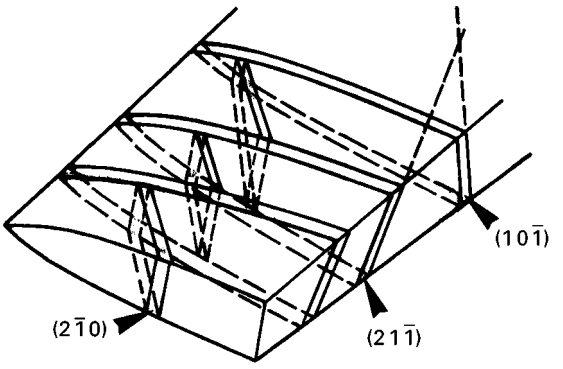

Figure 5 Schematic diagram showing the geometric configuration of the (2 1 1̄), (2 1̄ 0) and (1 0 1̄) twins in a γ martensite plate, which gave rise to the fringe contrast such as seen in Fig. 3b.

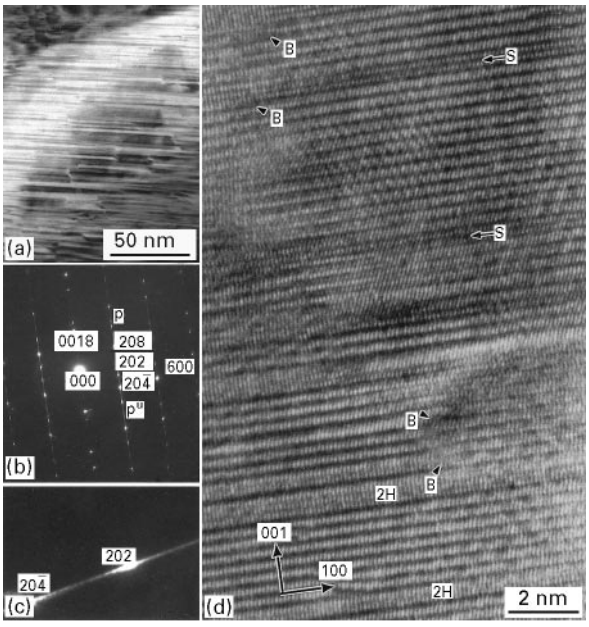

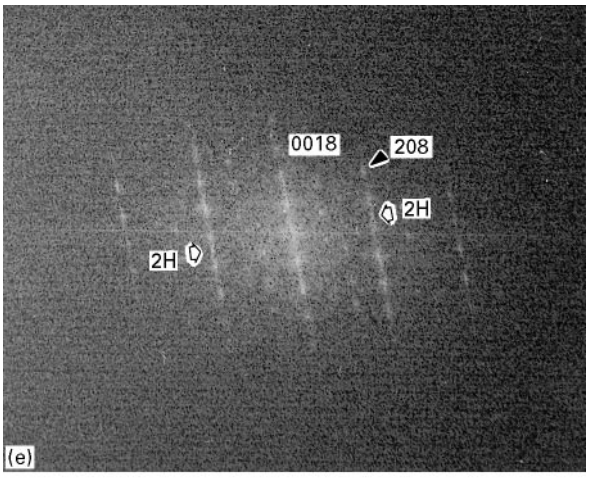

Figure 6 Martensite with stacking faults in a Cu–11.2 wt% Al–3 wt% Ni specimen quenched from 1173 K. (a) TEM bright field image of the martensite plate. (b) Electron diffraction pattern of the martensite in Fig. 6a, which is a [0 1 0] zone pattern of the ordered *N*9*R* structure with some reflections shifted along the [0 0 1] direction. (c) Enlargement of a part of the (0 1 0)* pattern. (d) A high resolution image of the martensite in Fig. 6a projected along the [0 1 0] orientation of the *N*9*R* structure. (e) Fourier transform of the atomic image in Fig. 6d.

(0 1 0) plane of the 9*R* structure. Thin bands of the 2*H* structure (marked 2*H* in Fig. 6d) are distributed in the plate as shown in this image. Each band is only several times the lattice spacing along the thickness.

Boundaries such as those indicated by the arrows labelled B, where the atomic lattice planes are displaced, are also revealed in this image. These boundaries seem to be antiphase domain boundaries.

An electron micrograph of this martensite projected along the [1 1 0] direction and its corresponding diffraction pattern are shown in Fig. 7a and b, respectively. The diffraction index of a segment of Fig. 7b is illustrated in Fig. 7c. Fig. 8a is an atomic structure image of the β_1' martensite, which is a segment of the image in Fig. 7a. Small domains about several nanometres in size are visible due to differences in contrast. The diffraction pattern (Fig. 7b) of this martensite plate is basically consistent with the [1 1 0] zone pattern of an ordered *N*9*R* structure, but some of the reflection spots are shifted along the [0 0 1] direction. For example, reflections with diffraction indices $h = 3n \pm 1$ are shifted as schematically represented in Fig. 7c. The [0 1 0] pattern in Fig. 6b also shows such spots shifting. These two patterns contain a series of such reflection spots, whose positions are shifted along the *c*-axis direction from the regular *N*9*R* reciprocal lattice points.

According to the theoretical analysis of Nishiyama *et al.* [9] and Kajiwara and Fujita [10], shifting of the diffraction spots in 9*R* type martensites is attributed to the stacking fault structure. The parameters of the probability of formation, α and β, for cubic and hexagonal type stacking faults can be derived from the shifting exhibited by the diffraction spots. For regularly ordered 9*R* structures, β equals zero. However, the fault probability, β, increases as the fraction of hexagonal type structure increases until, for 2*H* structures, the parameter becomes $\beta = 1$. In the present observation, the probability parameter, β, ranged from zero to one in the martensite plates. This implies that a "β" martensite plate usually possesses 9*R* structure with mingling of 2*H* structural domains. This is also verified by HREM examinations. Fig. 6e shows a Fourier transform (FT) of the high resolution image, Fig. 6d. Most spots of this FT pattern are consistent with the *N*9*R* structure, but some spots from the 2*H* structure also exist in the pattern, as shown by the arrow labelled 2*H*.

Furthermore, the diffraction spots in Figs 6 and 7 not only shift but also split into a few very weak small spots. An example is given in Fig. 6c. The shifting of some diffraction spots results from the existence of stacking faults, while the splitting of diffraction spots may be explained in the following way. Because of the existence of stacking faults and 2*H* thin bands with certain probability in a regular 9*R* structure, faults appear at an average interval of layers, m_s, of the basal (0 0 1) planes. The crystal can be considered as a regular 9*R* structure superimposed on a structure with longer periodicity. This periodicity is the average spacing, $m_s \times d_{001}$ of the stacking faults and 2*H* bands. Therefore, such a structure would give extra diffraction spots at n/m_s positions along the [0 0 1] direction. Here n is an integer.

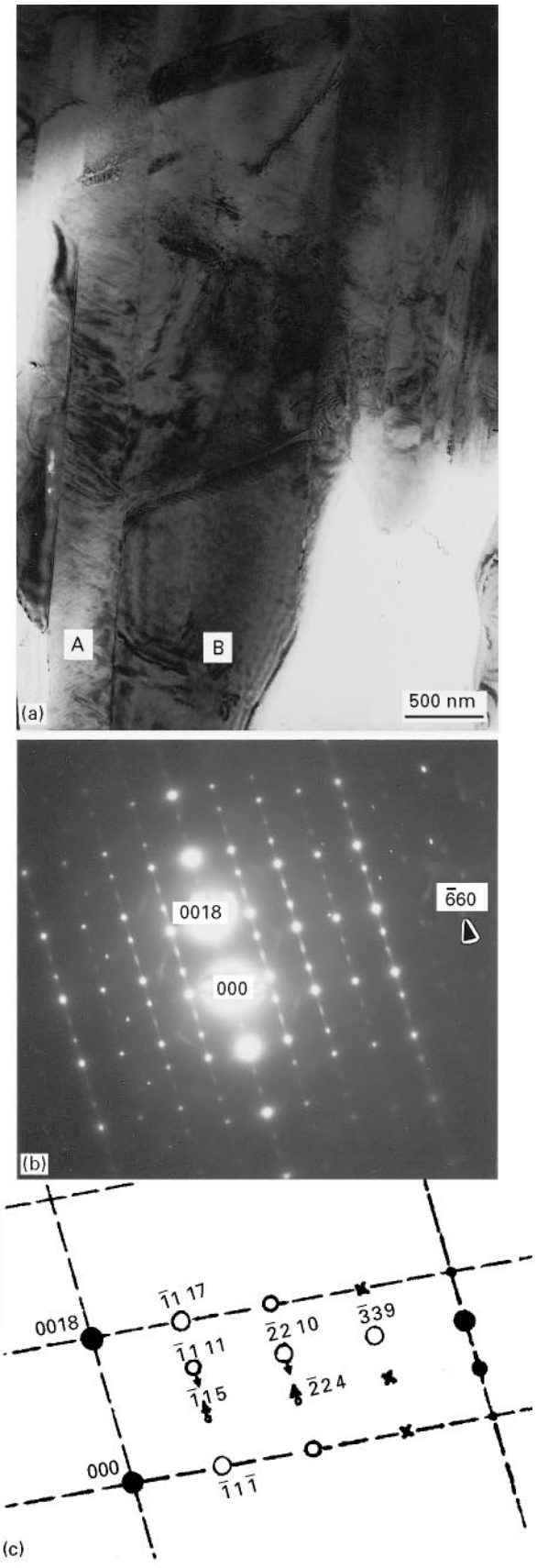

Figure 7(a) A martensite plate (B) with ordered *N*9*R* structure. (b) Diffraction pattern of plate B, which is the [1 1 0] zone pattern of the *N*9*R* structure. (c) Index of a part of Fig. 7b: (●) basic spots, (○) superlattice reflection, (×) forbidden reflection.

Contrast striations in a β_1' martensite plate projected along the $[1\,1\,0]_{9R}$ has also been observed by TEM. This is shown in Fig. 9b, which is an enlargement of the small part (AA) of Fig. 9a. The imaging

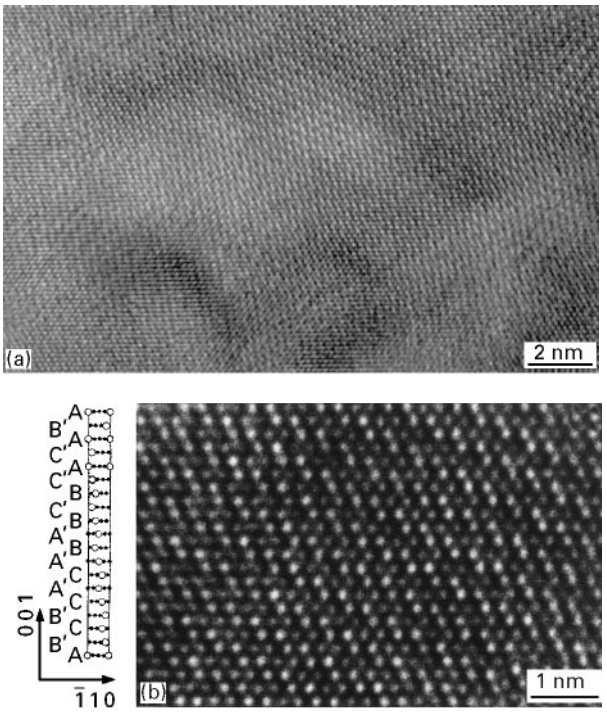

Figure 8(a) Atomic structure image of the ordered *N*9*R* martensite projected along the [1 1 0] direction. (b) A region of Fig. 8a at larger magnification accompanying the projection model of the ordered *N*9*R* unit cell along the $[1\,1\,0]_{9R}$ direction.

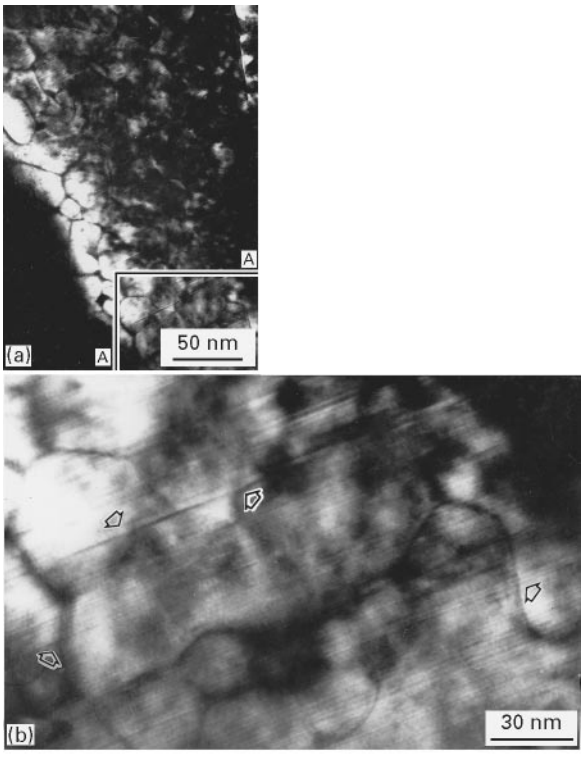

Figure 9(a) *TEM* dark field micrograph of a 9*R* martensite structure projected along the [1 1 0] direction showing contrast striations of the stacking faults. (b) Enlargement of part AA in Fig. 9a. Note that the faults cross the antiphase boundaries (as indicated by the arrows) of the martensite plate.

condition of Fig. 9b is the same as the high resolution image of Fig. 7 but at much smaller magnification. The fine fringes in the picture are stacking faults and thin bands of 2*H*. These are found across the whole martensite plate and are indicated by the arrows shown in Fig. 9. Coexistence of the 2*H* structure with the 9*R* structure within a martensite microtwin in a quenched Cu–14 wt % Al–4 wt % Ni alloy has also been observed by TEM by the present authors. Thus, the structure of martensite in the Cu–Al–(Ni) system cannot be identified merely by its morphology. A martensite plate may consist of small domains. These domains (thin bands) can possess different stacking structures due to local elastic strains and compositional variation in the specimen.

4. Conclusions

Two types of martensitic structures, i.e. γ'_1 and β'_1 martensites, coexist in the quenched Cu–11.2 wt % Al–3 wt % Ni alloy. The γ martensite structure seems to correspond with the monoclinic system rather than the orthorhombic system. Its lattice parameters deduced from both X-ray and electron diffraction data are: $a = 0.446$, $b = 0.540$, $c = 0.424$ nm and $\beta = 92^\circ$. This martensite is characterized by three microtwin variants with $\{1\,2\,1\}$, $\{2\,1\,0\}$ and $\{1\,0\,1\}$ twinning planes. A large number of microtwins exists within a single martensite plate resulting from accommodation of the transformation.

The microstructure of a β'_1 martensite plate in the same Cu–11.2 wt % Al–3 wt % Ni specimen is of *N*9*R* structure mixed with thin 2*H* domains. A large number of stacking faults exists in the plates. The parameters of the probability of faulting may be determined by shifting certain reflections in the diffraction patterns. This morphological feature characterizes the elastic strain energy effect arising from the volume and shape accommodation during martensite formation.

Acknowledgements

The electron microscope work was carried out at Okayama University of Science in Japan. The authors would like to thank Professors E. Sukedai and Y. Yokota for their valuable help and discussions. Thanks are also due to Mr Y. Makita for image processing. The project is partially supported by the National Natural Science Foundation of the People's Republic of China.

References

1. Z. NISHIYAMA, "Martensite transformation," (Maruzen Co, Ltd., Japan, 1971) p. 56–69.
2. C. M. WAYMAN, *Metal. Mater. Trans. A* **25A** (1994) 1787.
3. B. C. MUDDLE, J. F. NIE and G. R. HUGO, *ibid.* **25A** (1994) 1841.
4. J. W. CHRISTIAN, *ibid.* **25A** (1994) 1821.
5. K. SHIMIZU, in Proceedings of International Conference on Martensitic Transformations (ICOMAT-92), Monterey, July 1992, edited by C. M. Wayman and J. Perkins (Monterey Institute of Advanced Studies, CA, 1993) p. 13.
6. K. OTSUKA and T. OHBA, *ibid.* p. 221.
7. K. SHIMIZU and T. TADAKI, *Mater. Trans. JIM* **33** (1992) 165.
8. J. YE, M. TOKONAMI and K. OTSUKA, *Metal. Trans. A* **21A** (1990) 2669.

9. Z. NISHIYAMA, J. KAKINOKI and S. KAJIWARA, *J. Phys. Soc. Jnp* **20** (1965) 1192.
10. S. KAJIWARA and H. FUJITA, *ibid.* **21** (1966) 400.
11. F. C. LOVEY, G. VAN TENDELOO, J. VAN LANDUYT and S. AMELINCKX, in Proceedings of the International Conference on Martensitic Transformations (Nara, Japan, Inst. Metals, 1986) p. 762.
12. Z. NISHIYAMA and S. KAJIWARA, *Jpn*: *J. Appl. Phys.* **2** (1963) 478.
13. K. OTSUKA, C. M. WAYMAN, K. NAKAI, H. SAKAMOTO and K. SHIMIZU, *Acta Metall.* **24** (1976) 207.
14. K. OTSUKA and K. SHIMIZU, *Int. Met. Rev.* **31** (1986) 93.
15. P. R. SWANN and H. WARLIMONT, *Acta Metall.* **11** (1963) 511.
16. Y. S. SUN, G. W. LORIMER and N. RIDLEY, in "Phase transformation 1987", edited by G. W. Lorimer (Institute of Metals, Cambridge, UK, 1987) pp. 123–6.
17. S. EUCKEN, P. DONNER and E. HORNBOGEN, *ibid.* p. 174.
18. Q. JIANG, *Acta Metall. Sinica* **30** (1994) A49.
19. F. MARKETZ, F. D. FISCHER and K. TANAKA, *J. De Physique* **5** (1995) C2–537.
20. Q. JIANG, J. C. LI and J. TONG, *Mater. Sci. Eng. A* **196** (1995) 165.
21. A. D. COCKERILL, N. F. KENNON and D. P. DUNNE, in Procedings of the International Conference on Martinsitic Transformations (ICOMAT-92), Monterey, July 1992, edited by C. M. Wayman and J. Perkins (Monterey Institute of Advanced Studies, CA, 1993) p. 1071.
22. K. OTSUKA and K. SHIMIZU, *Scripta Metall.* **4** (1970) 469.
23. T. ICHIKAWA, N. OTANI, S. MIYAZAKI and K. OTSUKA, *ibid.* **23** (1989) 1329.
24. K. SHIMIZU, "in Phase transformations 1987", edited by G. W. Lorimer (Institute of Metals, Cambridge, UK, 1987) p. 272.
25. X. J. WU, F. H. LI and H. HASHIMOTO, *Phil. Mag. B* **63** (1991) 931.
26. H. HASHIMOTO, M. KUWABARA, Y. TAKAI, S. TSUBOKAWA and Y. YOKOTA, *J. Electron. Micrs. Tech.* **12** (1989) 180–200.
27. L. A. SHEPARD, in "Shape memory effects in alloys", edited by J. Perkins (Plenum Press, 1975) p. 421.
28. T. TADAKI, M. TOKORO and K. SHIMIZU *Trans. JIM* **16** (1975) 286.

Received 2 February 1995
and accepted 17 July 1996